From semisolid metal processing to thixotropic 3D printing of metallic alloys

Yifan Fei^a, Jie Xu^a, Donggang Yao^b, Jack Zhou^a*

^aDepartment of Mechanical Engineering and Mechanics, Drexel University, Philadelphia, PA, USA

^bSchool of Materials Science and Engineering, Georgia Institute of Technology, Atlanta, GA, USA.

Correspondence to: Jack Zhou, Department of Mechanical Engineering and Mechanics, Drexel University, PA, USA; Zhoug@drexel.edu.

From semisolid metal processing to thixotropic 3D printing of metallic alloys

Semisolid metal processing is a well-known technology that can be used to enhance manufacturing product quality in broad industries. The technology controls the thixotropic properties of alloys within their solidus and liquidus temperature ranges. In general, most known alloys can generate semisolid slurries at high solid fractions and the remaining can form slurries at low solid fractions. This has provided opportunities for many metals and alloys to be processed as semisolid slurries in today's casting industry. However, only a few researchers studied this technology potentially for a new metal-based additive manufacturing or 3D printing process. This article reviewed literature and findings from thixotropy rheology and semisolid metal processing methods, finally to thixotropic metal 3D printing. The survey shows that more future work is needed, including the investigation of thixotropic metal flow mechanics, the modeling and simulation of semisolid metal extrusion, and further development of a fully thixotropic 3D printing system.

Keywords: Thixotropic 3D printing, Thixotropy, Semisolid metal, Semisolid metal processing, Fused Deposition Modeling.

1. Introduction

Thixotropy is a rheological phenomenon and was first introduced in the early 1920s (Barnes 1997). This phenomenon can be found in many non-Newtonian pseudoplastic fluids such as paints, coatings, clays, food, gels, polymers, and metal slurries (Jan Mewis and Wagner 2009). Thixotropy was described as a time dependent property that is connected with the material's yield strength and viscosity. In the 1970s, the thixotropy of semisolid metal (SSM) was introduced, and the semisolid processing (SSP) technologies have since been changing the status of manufacturing industries (Kirkwood 1994). Semisolid metal processing integrates the advantages of traditional metal casting and forging, allowing to produce high quality complex metallic parts. In

the last three decades, on the other hand, additive manufacturing (AM) or 3D printing (3DP) has attracted widespread interest in fields such as product design, automotive manufacturing, aerospace, and bio-medical industries (Abdulhameed et al. 2019; Gao et al. 2015). Especially, metal 3D printing has received a fast growth since the 1980s, and some of the metal printing methods such as powder bed sintering, powder feed, and wire feed are now widely used in industry and academy (Ngo et al. 2018). However, powder-based laser melting or sintering methods for metal 3D printing are relatively expensive and are only applicable to a limited number of special metallic materials such as titanium alloy and stainless steel. Such laser sintering methods are technically not suitable or difficult to be implemented for processing of metallic powers that are covered naturally by a passivated oxidation layer such as powders from aluminum, zinc, magnesium, and their alloys. Accordingly, there emerges a need for the development of new metal printing methods that are cost effective, highly controllable, and suitable for processing a wide range of metallic materials. Using thixotropy property of semisolid metal and semisolid processing can be a possible solution for future metal 3D printing. In this paper, a literature survey is conducted on thixotropy and thixotropic metal processing on the basis of various research papers and reports published in related fields, with focused discussion on the use of thixotropy for metal 3D printing. The concept of thixotropy may provide a clear direction in design of new thixotropic metal printing systems. Traditional semisolid processes and related industrial SSP systems are surveyed, and their suitability for freeform metal extrusion is discussed. The paper also reviews new developments related to thixotropic metal 3D printing that have attracted increasing research interest in the recent years.

2. Thixotropy

Freeform fabrication (FFF) of metallic materials using an extrusion-based fusion process such as fused deposition modeling (FDM) would require the printing material to reach suitably high viscosity under certain controllable flow rate. One potential method for controlling the rheological properties of a metal fluid is to utilize the thixotropic behavior of semisolid metals. For better understanding of the relation between thixotropy and 3D printing, a brief account of thixotropy is provided first.

2.1. History of thixotropy

A survey of the early history of thixotropy has been given by Barnes (Barnes 1997). Then Mewis and Norman (Jan Mewis and Wagner 2009) gave a more recent review of thixotropy. Based on these two reviews, we here provide a brief history of developments in the field of thixotropy. In 1923, Schalek and Szegvari (Tanner and Walters 1998) observed that aqueous gels containing iron oxide can transform their states via certain physical methods. They particularly commented that these gels "have the remarkable property of becoming completely liquid through gentle shaking alone." Further experiments showed that these gels were able to transform from liquid back to gel after being left alone for a period of time, and this process can be repeated (Jan Mewis and Wagner 2009; Tanner and Walters 1998). In 1927, Peterfi coined the term thixotropy which is constructed from "thixis" and "Trepo", two Greek words (Peterfi 1927). In 1935, Freundlich and Röder studied the thixotropy phenomenon (Barnes 1997; Freundlich and Röder 1938), and Freundlich published a book entitled "Thixotropie". This is known as the first book in the name of thixotropy. In Freundlich and Röder's research, the authors particularly proposed a steady state model for the viscosity of thixotropic gels (Freundlich and Röder 1938; Tanner and Walters 1998).

Additionally, some researchers also considered Blair's study in 1942 on multiple materials is subject to thixotropy rheology (Blair and Coppen 1942). These studies and discoveries about thixotropy contrasted the traditional understanding in rheology at that time. Actually, a number of researchers proposed to separate thixotropy from classic Newtonian fluid mechanics (Tanner and Walters 1998). Nowadays, it's in a general agreement that the thixotropy terminology was originally introduced by Freundlich, and Peterfi was the first one discovered the thixotropic phenomenon. It is also interesting to mention that some time-dependent materials show behavior opposite to thixotropy; that is, the viscosity increases with time of shear at a constant strain rate or stress, but it gradually decreases when the shear flow ceases (Tanner and Walters 1998; Wei et al. 2019). Besides, it should be noted that the phenomenon of thixotropy has already been widely applied in the industry. One example is the formulation of building material in the construction industry. Clays or concretes with different recipes were produced to adjust the material's thixotropic behavior. Characterization of thixotropy can lead to better control of material's flocculation rate to achieve improved performance on formwork (Barnes 1997; Roussel 2006). High-thixotropy concrete becomes a suitable printing material that can be extruded by a 3D printer to manufacture large-scale structures (Zhang et al. 2019). Moreover, utilization of the thixotropy of alloys has led to notable innovations in the manufacturing industry. One example is thixomolding; as a special thixotropic casting method for aluminum and magnesium based alloys, thixomolding represents a relatively well-established industrial sector.

2.2. Concept and modeling of thixotropy

2.2.1. Definition of thixotropy and rheological properties

Despite the confusion on the early stage of research, researchers have reached a generic consensus on the description of thixotropy: "the continuous decrease of viscosity with time when flow is applied to a sample that has been previously at rest and the subsequent recovery of viscosity in time when the flow is discontinued" (IUPAC terminology) (Cotterill 2003; Jan Mewis and Wagner 2012). Nguyen and Uhlherr considered a material to be thixotropic if the viscosity or the related shear stress decreases at a constant shear rate (Nguyen and Uhlherr 1985). From these definitions, it is seen that a thixotropic material should exhibit reduced flow stress under a constant flow condition. An example of such a time-dependent behavior is shown in Figure 1 for a red mud suspension (Chhabra and Richardson 2011).

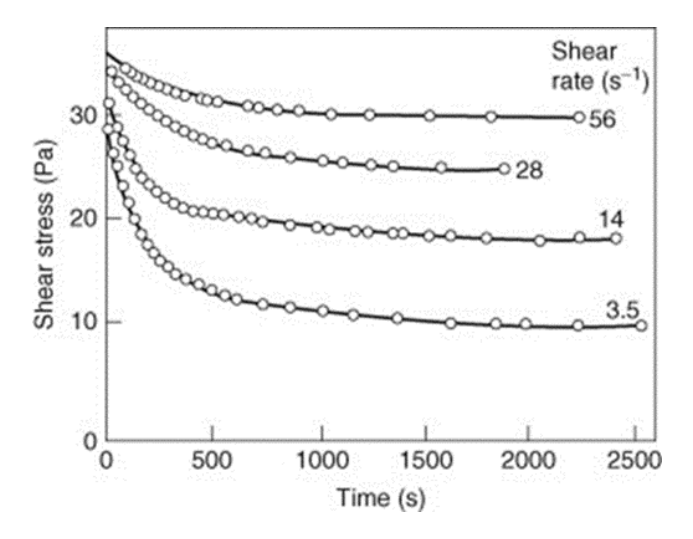


Figure 1. Time dependent relation of thixotropy for a red mud suspension (59wt% solid content) (Chhabra and Richardson 2011).

In a single testing experiment, the shear rate ramps up from 0 to the set value and subsequently decreases to 0 again. The flow curve of hysteresis loop can be measured from such a test. An representative plot of the hysteresis loop is provided in Figure 2

(Figure redrawn from Ref. (Chhabra and Richardson 2011)). The geometry and enclosed area of the hysteresis loop are known to be largely contingent upon the shear rate and the shear time, as well as the previous kinematic history of the testing material. Generally, if the hysteresis loop has larger enclosed area, the sample will have stronger time-dependent behavior (Chhabra and Richardson 1999; 2011).

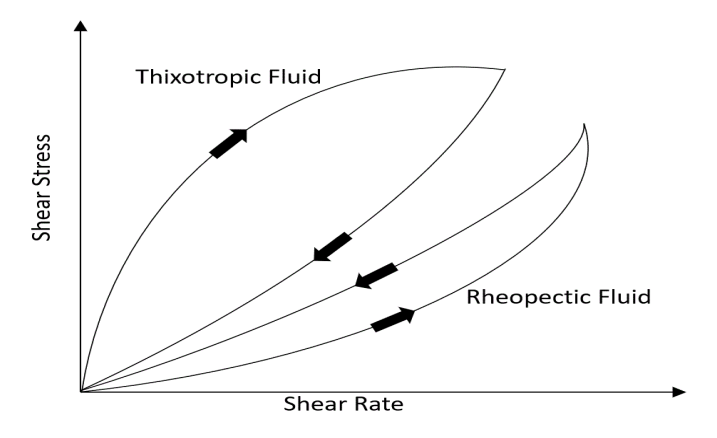


Figure 2. Schematic view of shear stress versus shear rate for thixotropic and rheopectic fluids. (Figure redrawn from Ref. (Chhabra and Richardson 2011))

When observing the macroscopic view of a thixotropy material, such as an aqueous particulate suspension shown in Figure 3, one can see that solid particles interact with each other and with the surrounding liquid medium so that a strong network structure is formed at a macroscopic scale (Darvell 2018). This three-dimensional structure can be formed from many physical forms of particles or fillers, including oriented fillers, coiled fibers, aggregated emulsions or agglomerated particles, and once destructed by shear it can be regenerated upon cessation of shear. The structure itself is fragile and unstable upon shear, and the resulting flow is controlled by the material's state of assembly. Figure 3a and 3b represent a molecular network that produces a gel state due to hydrogen bonding. This fragile structure can be destructed by applying continuous stirring. Once the stirring is stopped and the material is left at rest, the gel structure is

reformed, and the viscosity increases again. However, the structural re-formation cannot complete instantaneously within a short amount of time. Experiments have shown that the recovery process consumes time since slow intermolecular diffusion or inter-particle migration is involved during structural regeneration (Darvell 2018).

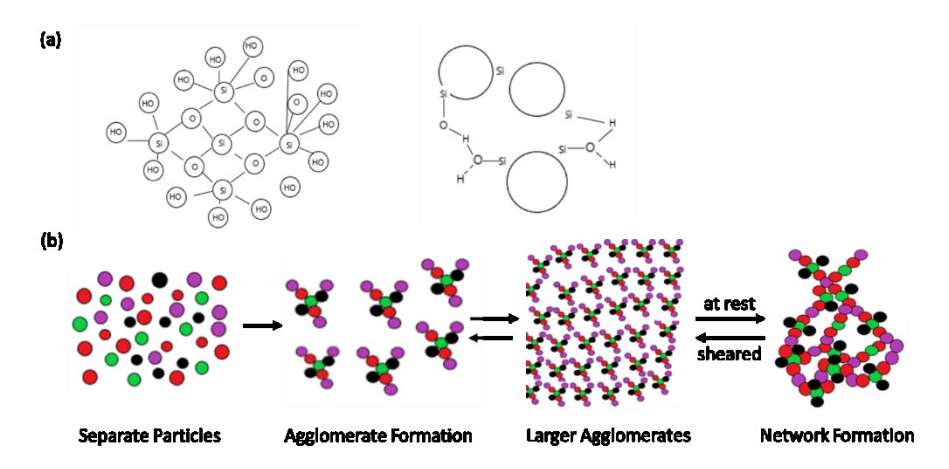


Figure 3. Example of the formation of thixotropy in an aqueous particulate suspension. Interparticle hydrogen bonding can cause the formation of a reversible gel network. (Figure redrawn from Ref. (Darvell 2018))

2.2.2. General thixotropy modeling

Larson and Wei (Larson and Wei 2019) defined an "ideal" rheological model for thixotropy which can be cast into a mathematical form of

$$\dot{\gamma} = \begin{cases} 0, & \sigma \leqslant \sigma_{y}(\lambda) \\ \frac{\sigma - \sigma_{y}(\lambda)}{\eta(\lambda)}, & \sigma > \sigma_{y}(\lambda) \end{cases}$$
 (1)

where the yield strength $\sigma_y(\lambda)$ and viscosity $\eta(\lambda)$ are dependent on λ , a "structural parameter" describing the state of structure of the material, that is, degree of agglomeration, strength of bonding, or status of jamming. Goodeve and Whitfield (CF Goodeve and Whitfield 1938) have presented a kinetic evolution equation for the structural parameter, namely,

$$\frac{d\lambda}{dt} = k_{+}(1 - \lambda) - k_{-}\dot{\gamma}\lambda\tag{2}$$

In this equation, both k_+ and k_- are the kinetic coefficients. In the simplest form, these two coefficients are constants, but in more general cases they can be expressed as functions of the shear rate. Term $k_+(1-\lambda)$ represents the structural development and $k_-\dot{\gamma}\lambda$ the structural breakage. The constant $1/k_+$ may be viewed as a thixotropic time scale τ_{thix} . The value of τ_{thix} defines the time that a material takes to attain a steady state after initiation of flow, or to regain an idle state after termination of flow. We can define a "thixotropy number", T_h ,

$$T_h = k_- \dot{\gamma} / k_+ = k_- \tau_{thix} \dot{\gamma} \tag{3}$$

which can be used to control the severity of thixotropy in flow, with low value of T_h indicating low thixotropy (Jan Mewis and Wagner 2009; Mujumdar *et al.* 2002). Solving the equation above in steady shear gives

$$\lambda = \frac{1}{1+T_h} + \frac{T_h}{1+T_h} \exp[-k_+(1+T_h)t]. \tag{4}$$

The constitutive equation linking stress with strain rate can be extracted from Equation (1). If the yield strength is exceeded, the equation can be transformed into

$$\sigma = \sigma_{\nu}(\lambda) + \eta(\lambda)\dot{\gamma} \tag{5}$$

In a simplified case, the viscosity and yield strength can both be assumed to be proportional to λ . Accordingly, a simple tensor equation for thixotropy can be obtained, as generalized by the following equation:

$$D = \begin{cases} 0, & \bar{\sigma} \leq \sigma_{y}(\lambda) \\ \frac{1}{2\eta(\lambda)} (1 - \frac{\sigma_{y}(\lambda)}{\bar{\sigma}}) (\sigma - \frac{1}{3} tr(\sigma)\delta), & \bar{\sigma} > \sigma_{y}(\lambda) \end{cases}$$
(6)

In this case, D is the deformation rate tensor $\left[D = \frac{1}{2}(\nabla v + \nabla v^T)\right]$, σ is the Cauchy stress tensor, δ is the identity tensor, and $\bar{\sigma}$ is an invariant of the stress tensor defined as

$$\bar{\sigma} \equiv \sqrt{\frac{1}{2} \left(\sigma - \frac{1}{3} tr(\sigma) \delta \right) : \left(\sigma - \frac{1}{3} tr(\sigma) \delta \right)}$$
 (7)

where the ":" symbol represents the scalar product of two tensors. Also, λ can fit into Equation (2) which is an evolution equation (Mujumdar *et al.* 2002).

In both Mewis's review (Joannes Mewis 1979) and Mewis and Wagner's review (Jan Mewis and Wagner 2009), the evolution equation for the structural parameter is considered a critical element in modeling of thixotropy. When modeling the kinetic model, these authors were inspired by classical kinetics in chemistry, so they considered the time derivative of λ to be linked with concurrent rates for structural formation and destruction. A general evolution equation for λ in this case can be cast into this form:

$$\frac{d\lambda}{dt} = -k_1 \dot{\gamma}^a \lambda^b + k_2 \dot{\gamma}^c (1 - \lambda)^d \tag{8}$$

where k_1 and k_2 are two rate constants for structural buildup and breakdown, and a, b, c and d are the powers that may be either obtained by data fitting or pre-assigned in the model. Nearly all existing evolution equations can be reduced to a generic format that reveals the major underlying physical processes (de Souza Mendes and Thompson 2012; Jan Mewis and Wagner 2009), namely,

$$\frac{d\lambda}{dt} = f_{peri}(\lambda) + f_{ortho}(\lambda, \sigma, \dot{\gamma}) + f_{rupt}(\lambda, \sigma, \dot{\gamma})$$
(9)

where f_{peri} represents forces caused by thermal motion and interparticle attraction (perikinetic aggregation), f_{ortho} is the orthokinetic aggregation, and f_{rupt} is the motion of rupture of bonds (CHARLES F Goodeve 1939; Kobelev and Schweizer 2005; Jan Mewis and Wagner 2009).

3. Semisolid metal processing

Previous research has shown that thixotropy establishes a comprehensive foundation relating material phase change with rheological properties. Nevertheless, thixotropy in metal was produced and observed about four decades behind the first discovery of thixotropy (Buschow *et al.* 2001). When metal is solidified, the microstructure is dendritic, as shown in Figure 4a, where a particulate structure is hard to observe. Only when the material reaches a semisolid state, the microstructure of metal starts to form "spheroids" or "globules", and weld or gap can be observed as the metal stays at rest (Figure 4b). When the material undergoes shear flow, the inter-spheroidal bonds have a tendency to break (Hashmi 2014). As shown in Figure 5, if the material undergoes constant shear for a long period of time, it will reach a plateau state (or equilibrium state) with a constant viscosity. This is considered to be associated with a distinctive aggregation size, and researchers have defined this equilibrium state as 'steady state.' A difference in the shear rate will produce a tendency toward a new plateau or equilibrium viscosity, which is linked with a new aggregation size (Hashmi 2014; Liu 2002).

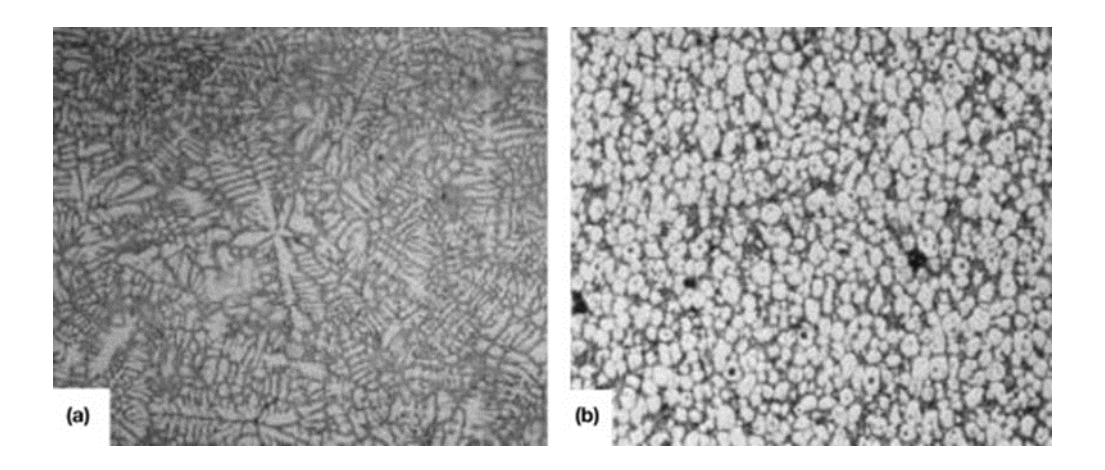


Figure 4. Solidified alloy structure: (a) dendritic microstructure typically observed in ascast samples; and (b) globular microstructure in semisolid alloy samples (Atkinson 2005).

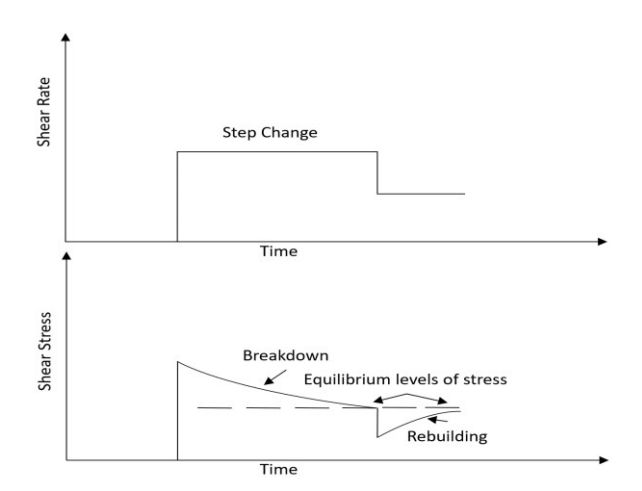


Figure 5. Evolution of shear stress for a thixotropic material subject to step changes of shear rate. (Figure redrawn from Ref. (Barnes et al. 1989))

From the literature survey conducted by Flemings (Merton C Flemings 1991), it is known that the processing of semisolid metal was originally cultivated as part of research at the Massachusetts Institute of Technology (MIT) in the 1970s. In the MIT experiment, alloy was set and stirred during solidification. The stirring process causes a significant change of internal structure which can lower the apparent viscosity of the slurry (Merton C Flemings 1974; 1991). Joly and Mehrabian in 1976 also observed that

the apparent viscosity is strongly dependent on the shear rate and the cooling history, as well as the solid fraction of the slurry (Figure 6) (Joly and Mehrabian 1976).

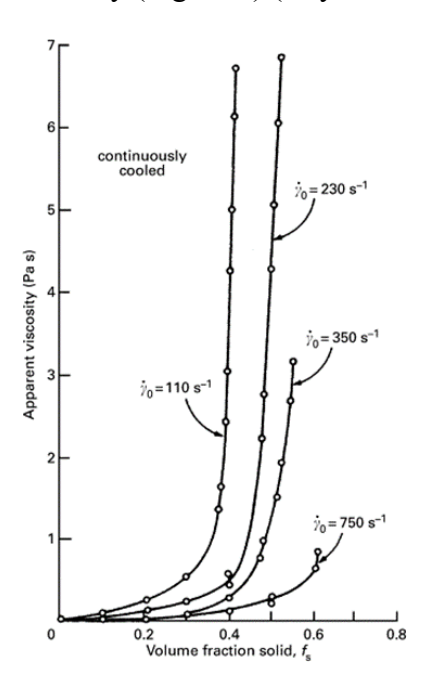


Figure 6. Apparent viscosity vs. fraction solid (fs) of Sn–15 wt.% Pb sheared continuously and cooled at 0.33 K/min at different shear rates (after Joly and Mehrabian 1976) (Merton C Flemings 1991; Joly and Mehrabian 1976).

It was found that when a semisolid alloy with certain fraction solids undergoes high shear rates and low cooling rates, substantial decrease in viscosity (1 Pa·s) of alloy slurries is achieved. Even with increase of the fraction solids to around 0.6, such relation is visible. Experimental observations show that external mechanical excitation such as shear during the solidification process can significantly alter the solidified structure from a dendritic structure to varied rosette forms and finally to spheroidal forms with the change of time (Buschow *et al.* 2001). As shown in Figure 4 above, in a liquid matrix, spheroidal solid particles can easily move around. For hydrodynamic reasons, this movement is much easier than that of the dendritic solid under same volume fraction. Figure 7 illustrates evolution of thixotropic properties of Sn-Pb slurries during multiple shear rates. The apparent viscosity of the slurry at a constant solid

fraction is time dependent, and should the sheared slurry be left at rest, the viscosity would increase substantially, typically by orders of magnitude. After the stirring process is restored, the viscosity will decrease again.

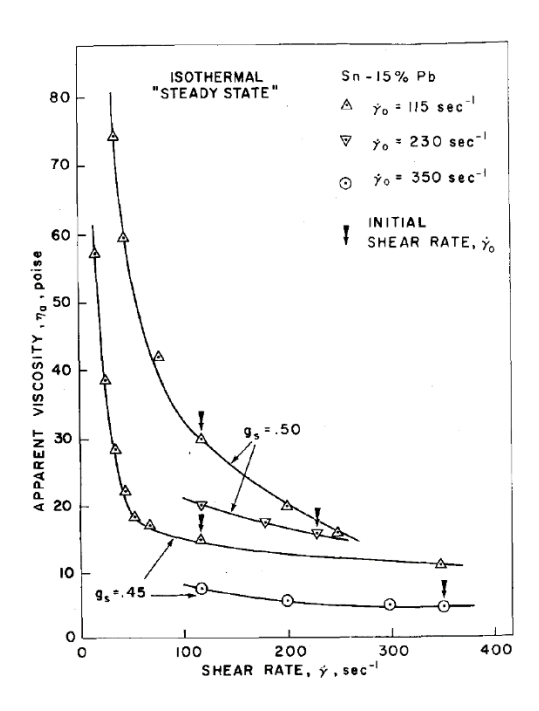


Figure 7. Apparent viscosity of Sn–15% Pb slurries under different shear rate ($\gamma = 115$ s–1,(γ) =230 s–1, and $\gamma = 350$ s–1). Samples were shared then kept at solid fraction of 0.45 and 0.50. (Joly and Mehrabian 1976).

Flemings also mentioned that the above behavior is physically reversible and is related with the clustering or aggregation of solid particles when the degree of shear is decreased, and such clusters break up and separate when shear is started again (Merton C Flemings 1991). In their literature review, Polmear et al. summarized the advantages for semisolid processing (Polmear et al. 2017):

1. Semisolid processing significantly lowers "capital investment and operating costs when compared with conventional casting methods. The whole process can be contained within one machine so that the need for melting and holding furnaces as well as melt treatment are all avoided. Foundry cleanliness is easy to maintain, and energy

requirements are less because complete melting is not required, cycle times are reduced, and scrap is minimized".

- 2. "Shrinkage and cracking within the mold are reduced because the alloy is already partly solidified when cast".
- 3. "Lower operating and pouring temperatures lead to an increase in the life of metal dies".
- 4. "Composite materials can be readily produced by adding fibers or other solid particulates into the feedstock" (compo casting).

3.1. Key parameters of semisolid metal

To understand the process variables and process parameters of metal, Püttgen et al. (Püttgen et al. 2007) have conducted research on thixotropic processing using steels as an example. In their study, fraction solid content is the crucial parameter to improve the thixoformability of steels. This explains that steels usually exhibit a large semisolid interval at low processing temperature, and low thermal sensitivity can provide a more stable process. Using DTA-measurements or thermo-dynamical calculation, the fraction liquid/fraction solid content and the thermal sensitivity S^* of the phase fractions of steels can be determined (Uggowitzer et al. 2000):

$$S^* = \frac{df_{1/s}}{dT} \tag{10}$$

where $f_{1/s}$ represents amount of liquid/solid phase and T is temperature. Regarding the breadth of the semisolid interval, pure iron and nearly eutectic alloys are excluded in their applicability (Püttgen *et al.* 2007).

For the microstructure of semisolid slurries, the effective parameters are the solid fraction, the particle size, the particle shape, and the particle distribution. These

parameters are normally determined on surfaces of quenched samples using standard metallographic techniques (Tzimas and Zavaliangos 2000; Underwood 1970).

For deliberate examination, time-taking serial sectioning is necessary to obtain the network structure that is formed in the material. Shape factor defined by the following equation can be used to describe the roundness of particles:

$$F = 4\pi \frac{A}{U^2} \tag{11}$$

where A is the area and U is the perimeter. For globular grains, F is equal to one. Otherwise, the value of F is between zero and one.

To describe the state of coalescence or interconnection of the solid particles, one can define a new parameter Cf_s to quantify the contiguity of the solid phase for the solid fraction (Nishimatsu and Gurland 1958), that is,

$$Cf_s = \frac{2Sv^{ff}}{2Sv^{ff} + Sv^{fs}} \tag{12}$$

where Sv^{ff} refers to the solid-solid interface, and Sv^{fs} refers to the solid-liquid interface. When Cf_s is equal to zero, all solid particles are enclosed by a continuous liquid phase (Püttgen *et al.* 2007). The whole amount of the coalesced solid phase is given by the volume contiguity of solid particles (Omar *et al.* 2005):

$$C_s f_s = V_s C f_s \tag{13}$$

where V_s is the solid volume, and Cf_s is the contiguity of the solid fraction. If the value of volume contiguity is greater than 0.3, thixotropy cannot be developed, and the material state is close to full solid. If the volume contiguity is smaller than 0.1, the aggregated skeleton of solid particles is not sufficiently strong to withstand the material

from deforming prior to the material's forming step; in this case, the state of material is closer to liquid which causes poor semisolid processability of the material (Omar *et al.* 2005).

3.2. Simulation of semisolid metal

A variety of semisolid metals are being tested and simulated from different perspectives. Particularly, Canyook et al. have characterized the microstructure of semisolid metal slurries during the early formation stages (Canyook et al. 2012). In their experiment, 356 aluminum alloy was chosen as the testing material, and they used a gas-induced semisolid (GISS) process to prepare samples during cooling. With the support of an image analysis system, the particle distribution within the sample can be distinguished and then converted to a solid fraction (Figure 8).

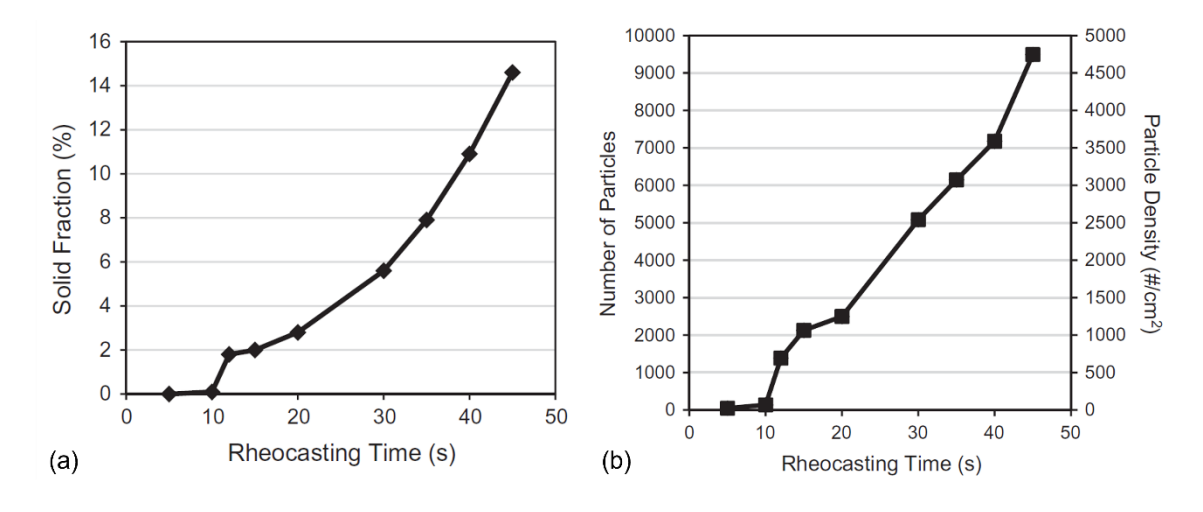


Figure 8. (a) Solid fraction of 356 aluminum alloy at different rheocasting times. (b) Total solid particles and the related particle density at different rheocasting times. (Canyook et al. 2012)

Prior to Canyook et al.'s research, Modigell and Koke presented a computer simulation of numerical flow for semisolid slurry (Modigell and Koke 1999). A tin-lead alloy (Sn-15%Pb) within a concentric cylinder rheometer was simulated by software FLOW-3D,

and the model was implemented at a fixed solid fraction of 0.5. The simulated flow behavior for selected SSM materials are reproduced in Figure 9. For comparison purposes, transient flow of Newtonian fluid is also included in the figure.

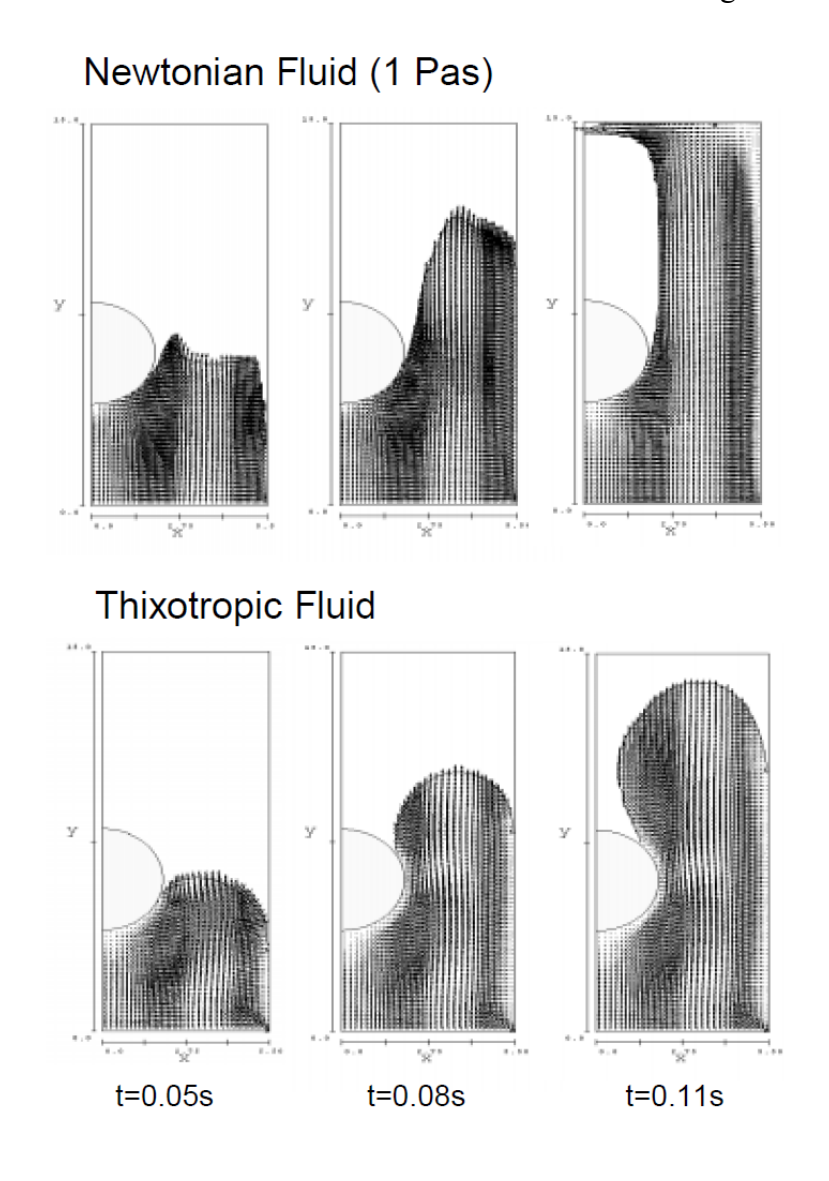


Figure 9. Simulation results of a casting process with a Newtonian fluid and a thixotropic non-Newtonian fluid (Modigell and Koke 1999).

3.3. Methods for generating grains in SSM

There are several innovative ways to use combined thermal and mechanical control to refine grains during melt processing, which have typically been employed to engineer the feed material for semisolid processing. Kaufmann and Uggowitzer divided these

methods into three major parts (Kaufmann and Uggowitzer 2001; Kaufmann *et al.* 2000):

- 1. "Use of chilled surfaces and melt temperature control, e.g., lower casting temperatures".
 - 2. "Shearing of melts while the melt is semisolid".
 - 3. "Conditioning of melts before solidification".

Figure 10 illustrates three methods for producing nondendritic structures (Merton C Flemings 1991). Batch stirring and continuous stirring within an extruder require physical contact with materials, and additional heating elements are applied to keep the desired temperature. In comparison, electromagnetic stirring, a widely used process in metal casting, can combine heating and stirring into one single process.

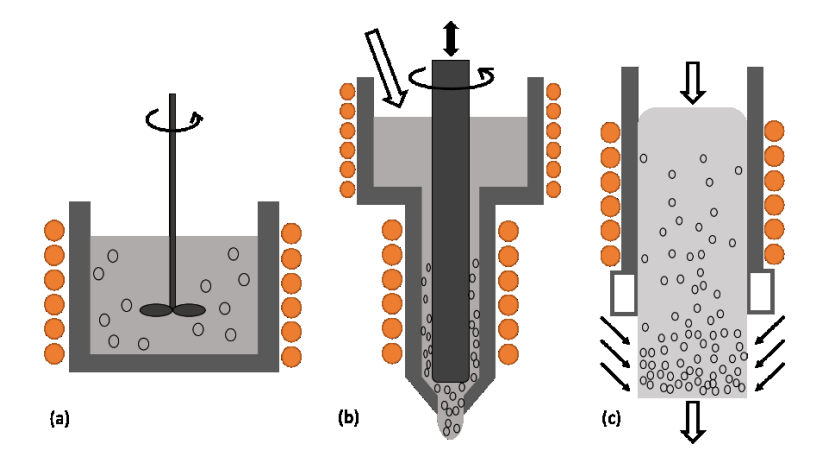


Figure 10. Schematic diagrams of methods for producing nondendritic structures: (a) batch stirring, (b) continuous stirring and extrusion, and (c) electromagnetic stirring with continuous casting. (Figure redrawn from Ref. (Merton C Flemings 1991))

Semisolid metal processing, in terms of the stirring state of materials, can be categorized into two major groups: rheocasting and thixoforming (Mohammed *et al.* 2014). Rheocasting starts with the liquid state of metal and then produces an SSM slurry with spheroidal microstructure which can be directly injected into a mold or die for

shaping without additional intermediate stage. Thixoforming, on the other hand, requires an intermediate stage before injection. When generating the intermediate state, the molten metal is solidified to form a billet. Then the metal is reheated and partially melted to form the semisolid state with a non-dendritic structure, and pressure-injected into the mold for component forming (Fan 2002).

3.3.1. Rheocasting

In Flemings' early research (MC Flemings *et al.* 1976), rheocasting was described as a basic process in which a highly fluidic, semisolid, nondendritic slurry is directly cast into a shape (Figure 11). Later, Mohammed *et al.* (Mohammed *et al.* 2013) developed a direct partial melting process for creating a nondentritic structure for theocasting. In general, the early-stage work in rheocasting mainly involved the use of mechanical stirring (such as the setup shown in Figure 11a) to obtain a globular microstructure, whereas recent work focuses on improvement of part quality and process efficiency (Atkinson 2005).

One example process of rheocasting is the new MIT process, also referred to as the cooling slope technique or liquids casting technique (new rheocasting (NRC))(de Figueredo 2001; Mohammed *et al.* 2013). In this new process of rheocasting (illustrated in Figure 12A), a molten alloy is poured into a vessel and reaches a uniform temperature just above the liquidus temperature. After a series of adjustments, the resulting metal slurry is finally pushed into the holding mold to keep the inside non-dendritic microstructure and finish the casting process.

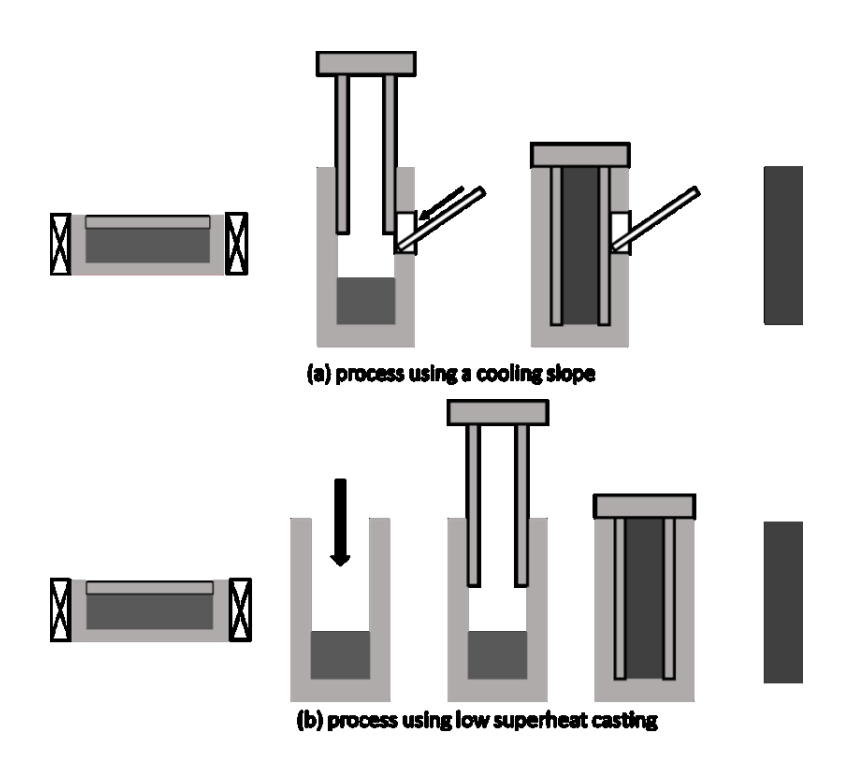


Figure 11. Rheocasting processes: (a) process using a cooling slope, and (b) process using low superheat casting. (Figure redrawn from Ref. (Haga and Kapranos 2002))

3.3.2. Thixoforming

In thixoforming, a solidified metal billet containing a globular microstructure is reheated to a semisolid state for mold forming (de Figueredo 2001; Mohammed *et al.* 2014). Common thixoforming processes can be divided into two types: thixoforging and thixocasting.

Thixoforging can be considered as a type of closed-die forging processes. After reheating the billet, the content of the liquid fraction of the metal prior to forming is relatively high (Ji *et al.* 2002; Kopp *et al.* 2001). As showed in Figure 12B, the reheated billet is directly placed in a forging die and while maintained in a semisolid slurry state, forced into the whole inside volume of the die.

Thixocasting has a similar reheating process but requires a different temperature range for the material. Usually, the semisolid billet has a liquid fraction of less than 50%.

During thixocasting, a plunger is used to insert the material into the lower half of a

horizontal open die. The two-piece die is then closed to force the material into the die cavity and produce a near net-shape component in a one-step operation (Figure 12B) (Kopp *et al.* 2001; Mohammed *et al.* 2014; Quaak *et al.* 1996).

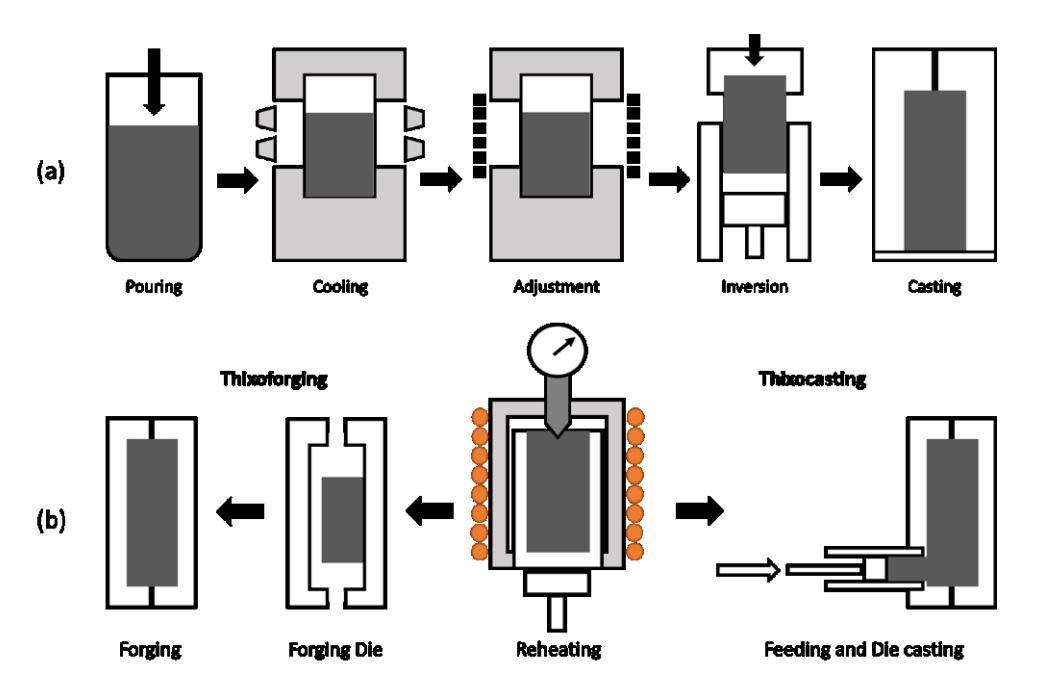


Figure 12. Schematic of (A) rheocasting method and (B) thixoforming method. (Figure redrawn from Refs. (Fan and Chen 2002; Kirkwood 1994; Kumar *et al.* 2019))

4. Direct metal deposition method and thixotropic metal 3D printing

SSM processing as a traditional manufacturing method may provide valuable opportunities for metal 3D printing. One widely used thixoforming processes in the industry is thixomolding, a process similar to the plastic molding process but uses a metallic feedstock material that contains a globular morphology. The design of a typical thixomolding machine is shown in Figure 13, including several key mechanisms such as material feeding, rotational plastication, and high-pressure extrusion and injection. It would be interesting to know if these mechanisms may be adapted to an extrusion-based metal 3D printing system.

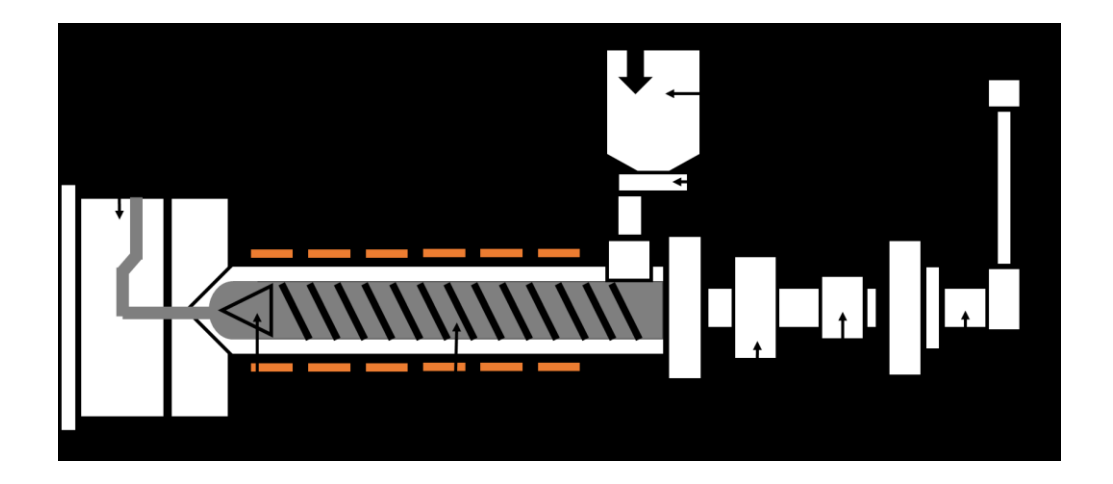


Figure 13. Schematic of a thixomolding machine for producing injection molded magnesium alloy components. (Figure redrawn from Ref. (Polmear *et al.* 2017))

Current metal 3D printing methods focus on transformation of metal powders into desired shapes. Methods like powder bed systems or powder feed systems are common for freeform fabrication of metallic components. These methods, however, require complex operating techniques and the resulting printing cost is high (Frazier 2014). In contrast, extrusion-based 3D printing techniques, considered to be more cost-effective, are widely used in printing polymers and other nonmetallic materials. In recent years, the FDM process has received increasing attention in metal 3D printing. The primary challenge is that a typical molten metal/alloy does not possess the desired fluidity for fusion deposition. Accordingly, some researchers choose to develop a semisolid metallic feedstock for fusion deposition, in order to achieve better material flow and process stability (Riecker *et al.* 2016).

Most wire-feeding systems fabricate filament using nonmetallic composites as a binder. Metal powder is combined with binder polymers to produce the feedstock. A filament is generated via an extrusion process and can be used in conjunction with an FDM system for 3D printing. However, printed geometries require additional steps including debinding and sintering (Wagner *et al.* 2021). In contrast, the feedstock for thixotropic

metal printing is exclusively composed of metallic materials. The two major preparation methods are as follows: one involves using preformed nondendritic metal filaments, and the other involves stirring molten metal to generate a thixotropic slurry. The direct metal printing system is compatible with metal filaments and thixotropic slurries (Jabbari and Abrinia 2019). Depending on the feedstock properties, the critical parameters for the thixotropic printing process include material solid fraction, processing temperature, feeding mechanism, and processing pressure (Chen *et al.* 2017; Jabbari and Abrinia 2018). The related work in this direction is surveyed in this section.

4.1. Fused coating based additive manufacturing (FCAM) method

Fang et al. (Fang *et al.* 2016) have investigated a fused coating based additive manufacturing (FCAM) method for direct deposition of molten metal layer by layer. In their process, as illustrated in Figure 14, a molten alloy is transferred from a fused-coating nozzle to the receiving substrate. A thermal capillary zone is developed between the nozzle head and the substrate. The molten alloy spreads into a subcylindrical or oblong shape under the combined influences of pressure, viscosity and surface tension. In this process, continuous pressure serves as the primary driving force for printing, coupled with the effect of an exhauster controlled by a frequency converter and a solenoid valve.

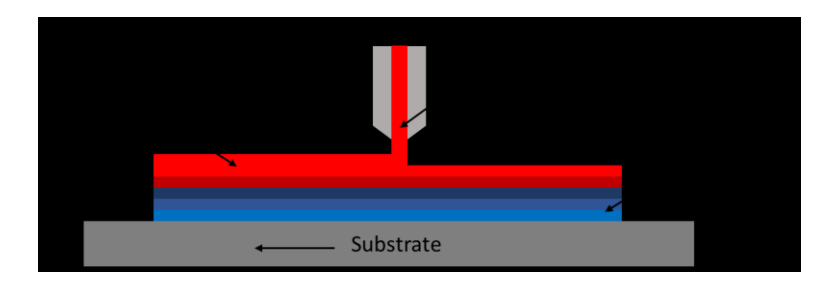


Figure 14. Principle of fused-coating based AM. (Figure redrawn from Ref. (Fang *et al.* 2016))

The frequency converter and solenoid valve are necessary for controlling the formation and termination of molten metal. The fused coating nozzle specially designed with a specified cone angle is used to assist in production of dense metallic components (Figure 15). Fang et al. claimed that the FCAM process has the potential in fabricating metallic materials, such as Sn/Pb alloy, aluminum alloy, copper alloy and even steel.

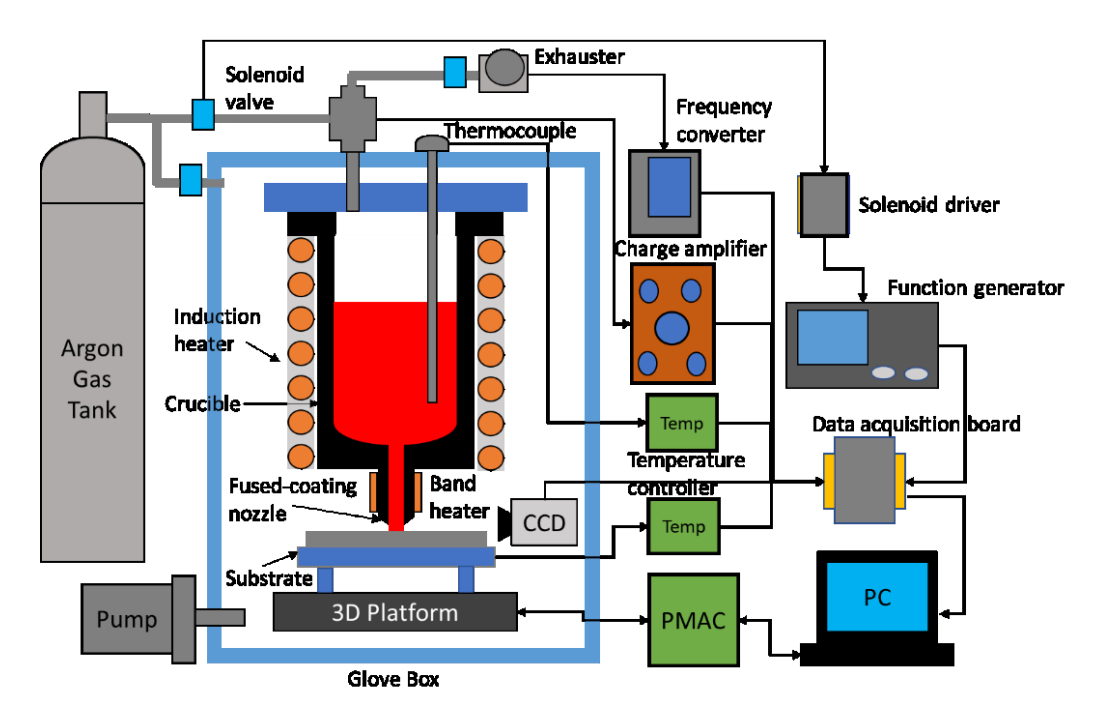


Figure 15. Schematic diagram of fused-coating based AM. (Figure redrawn from Ref. (Fang *et al.* 2016))

In their experiment, Fang et al. chose Sn63Pb37 alloy as a raw material. The material was melted in the molten metal generator. The generator includes a graphite crucible that is surrounded by an induction coil. A heated fused-coating nozzle is located at the bottom of the crucible through a threaded connection. The nozzle contains a detachable tip that connects the main body by threads. The nozzle contains a removable nozzle tip for easy assembly and disassembly. A 700W band heater wraps around the nozzle, and a thermocouple is inserted into the nozzle body to monitor the nozzle temperature.

Figure 16 shows some printing samples from the FCAM process.

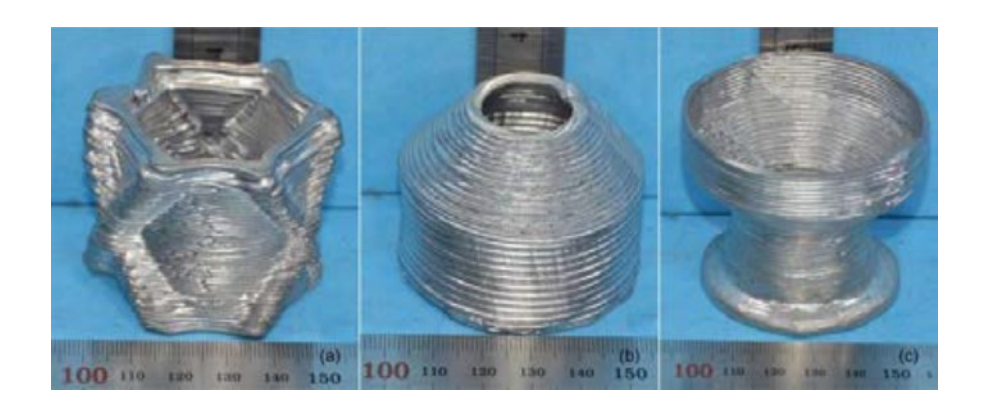


Figure 16. Metal parts fabricated by FCAM process. (Fang et al. 2016)

4.2. Semisolid metal extrusion and deposition (SSMED) process

Jabbari and Abrinia (Jabbari and Abrinia 2018) developed a semisolid melt extrusion and deposition (SSMED) system. The idea of this system originates from freeform additive manufacturing of polymers by fused deposition modeling. The system comprises a combination of a motion system, a feeding mechanism, and a heating source. The motion system employed in this research is a Cartesian robot-like FDM machine. The head for thixotropic extrusion of metallic filaments is mounted on the carriage of a three-axis table.

In Jabbari and Abrinia's experiment, cast billets were extruded through a single-step cylindrical extrusion die to decrease the diameter and produce a filament to be used as the feedstock material for the thixotropic extrusion process. The extrusion ratio was set to approximately 70 at room temperature. Billets of 25 mm diameter were extruded into 3-mm-diameter filaments on a 100-Ton hydraulic press. The extruded filaments were warmed up to 40°C due to large plastic deformation of 98% reduction in area. The ram speed was set at 4 mm/min to avoid extra heat generation. The extrusion die set, deformation zone, and produced wire are illustrated in Figure 17.



Figure 17. The extrusion dies set (left), deformation zone (up right), and produced wire (down right). (Jabbari and Abrinia 2018)

As shown in Figure 18, a 60-W nozzle heater element is used to surround the cylindrical hot end block. The amount of slurry in the liquefier is expected to depend on the heat flux and the filament feed rate, and this is considered to be one of the most important design criteria for the extruder. The heat barrier, made of stainless steel, is found to be a good solution acting as the main physical limit to prevent heat conduction into the upper part of the extruder. An annular heat sink is also designed and built above the heat barrier to minimize the heat conduction into the cold end and feeder mechanism. The heat sink material is made of aluminum alloy just like the material for the liquefier to enable maximum rate of heat exchange. Figure 19 displays several printing samples from this SSMED machine.

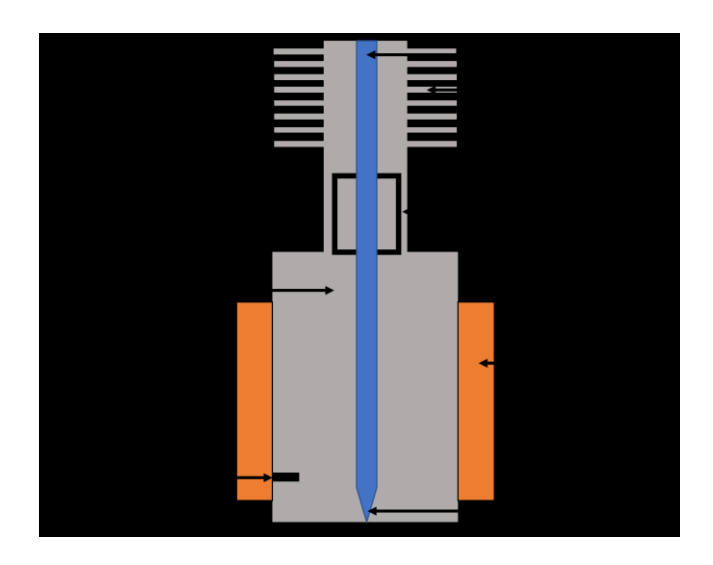


Figure 18. Schematic diagram of Developed SSMED thixo-extruder. (Figure redrawn from Ref. (Jabbari and Abrinia 2018))

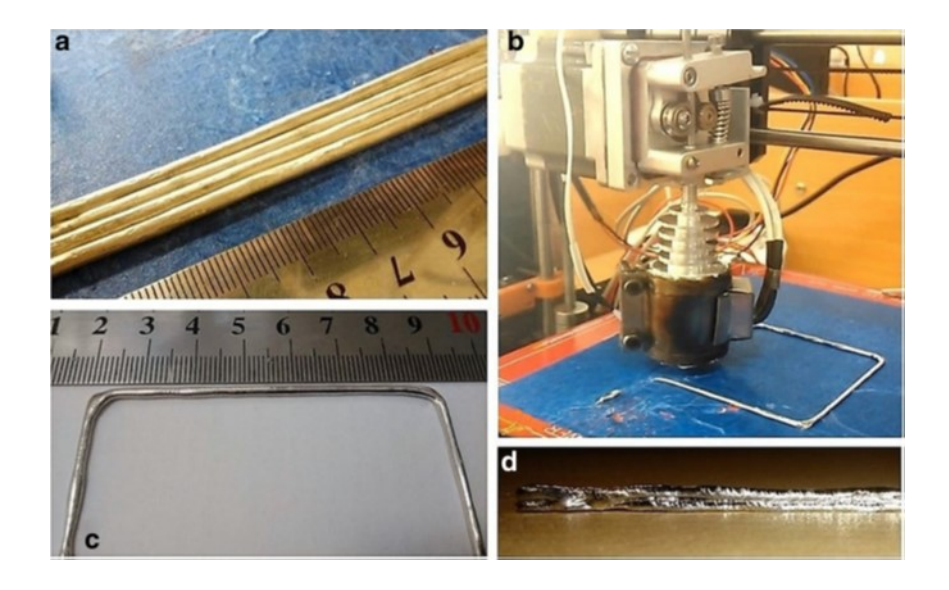


Figure 19. Deposited layers of semisolid alloy. A) Four layers printed adjacent to each other. B) Thixo-extruder printing a sample. C) A printed single layer square shape. D) A three layers printed sample. (Jabbari and Abrinia 2018)

4.3. Direct metal writing (DMW) method

Chen et al. introduced an alternative low-cost approach for AM of metal alloys (Chen *et al.* 2017). This method is established on the basis of direct metal writing (DMW) of metallic alloys in the semisolid state through controlling the microstructure and the

rheological behavior of semisolid alloy slurries. In their study, Chen et al. produced a proof-of-concept DMW prototype by using a simple and low temperature Bi-Sn binary semisolid alloy system as a representative example (Apelian *et al.* 2002; Lashkari and Ghomashchi 2007; Pan *et al.* 2004).

A rod-shaped ingot of 15mm diameter with a nominal composition of Bi75Sn25 was used as a printing material. The ingots were generated by arc melting and casting high purity (>99.99%) raw elements under an argon atmosphere (Figure 20). The solidus temperature (Ts) and the liquidus temperature (Tl) of the alloy ingots were identified by differential scanning calorimetry (DSC) to be 139°C and 225°C at a heating rate of 10°C/min, respectively. The alloy ingots were cut into pieces and fed into the DMW system, which is composed of a reservoir with an extended nozzle, a nitrogen pressure source, and a printing substrate.

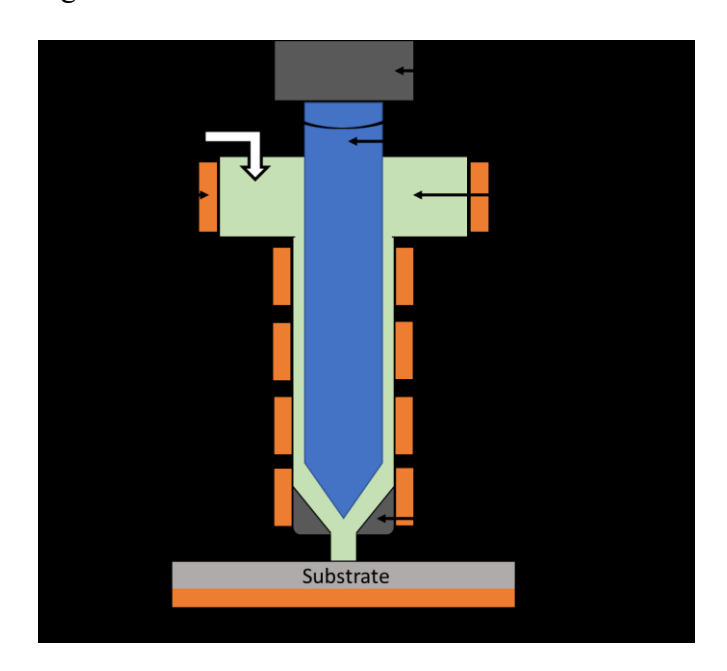


Figure 20. Schematic diagram of the DMW system comprised of an upper reservoir with an extended nozzle and a bottom printing substrate. A motor driven grooved spindle is inserted in the center of the nozzle to apply shear force to the semisolid alloy. (Figure redrawn from Ref. (Chen *et al.* 2017))

Resistance heaters with attached proportional integral differential (PID) controlled thermocouples were used to heat the semisolid alloy with a precision of 62°C. DMW in this case relies on the rheological properties that are mechanistically determined by the microstructure of the semisolid alloys.

For steady state DMW, a varied nitrogen pressure up to 0.6 MPa was applied into the reservoir to accommodate different viscosity at varying printing temperature and shear rate at a typical printing speed of 5 mm/s. For example, the two representative cases of DMW printed Bi75Sn25 structures were obtained under two different processing conditions. Figure 21 illustrates the printing results with different printing temperature.

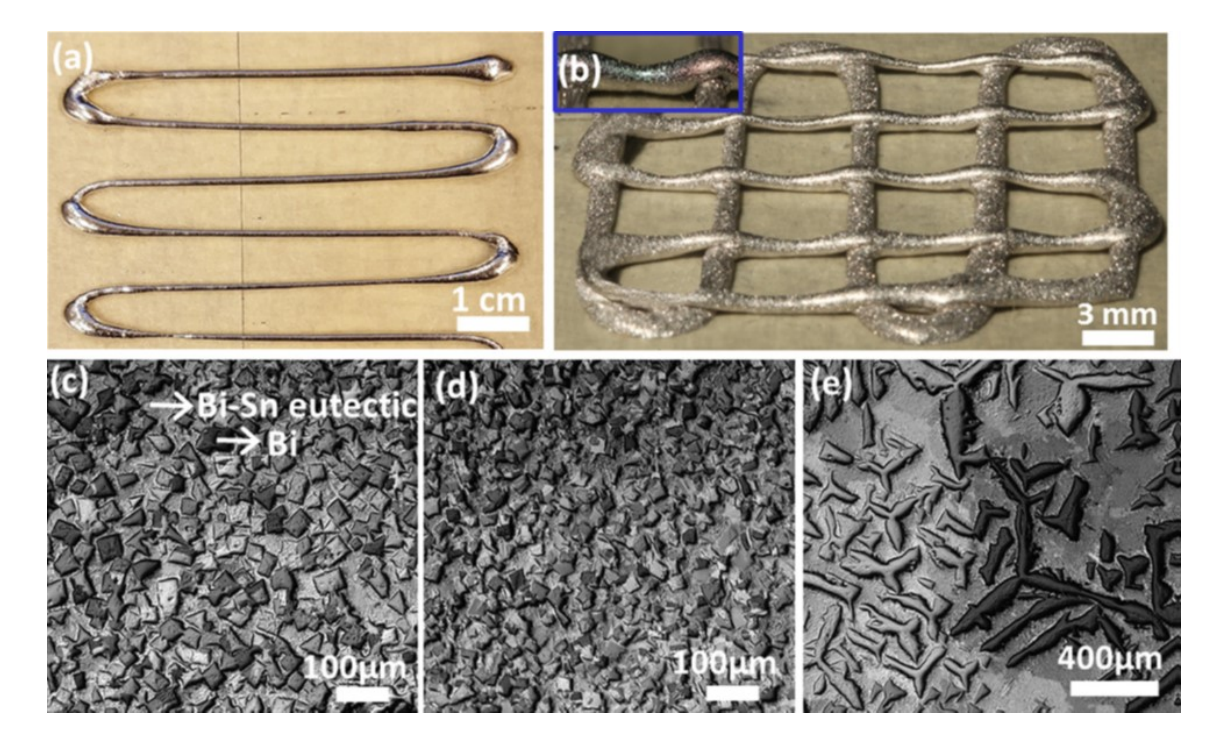


Figure 21. DMW fabricated Bi75Sn25 structures and their microstructures. The characteristic feature size of the filament is close to the nozzle size. (a) "Zigzag" pattern printed at 200°C. (b) Two layered lattice structure with overhanging features (blue inset) printed at 190°C. (c) and (d) Filament microstructures of prints (a) and (b), respectively, exhibiting a mixture of polygonal Bi blocks and the Bi-Sn eutectic matrix. (e) A Bi75Sn25 filament printed at 200°C without shear. Many long need-like dendrites tend to clog the nozzle and hence prevent steady state printing. (Chen *et al.* 2017)

4.4. Fused filament fabrication (FFF) method

Dalton et al. developed a novel additive manufacturing method inspired by the FDM process to fabricate Mg-Zn alloys (Lima *et al.* 2020). In their experiment, the printer setup is modified based on a Prusa 3D printer. Figure 22 shows that pre-produced alloy filament is feeding through the channel and then melted inside the nozzle head. The redesigned print head can hold the maximum working temperature around 700°C, which is compatible with printing median-melting temperature alloys.

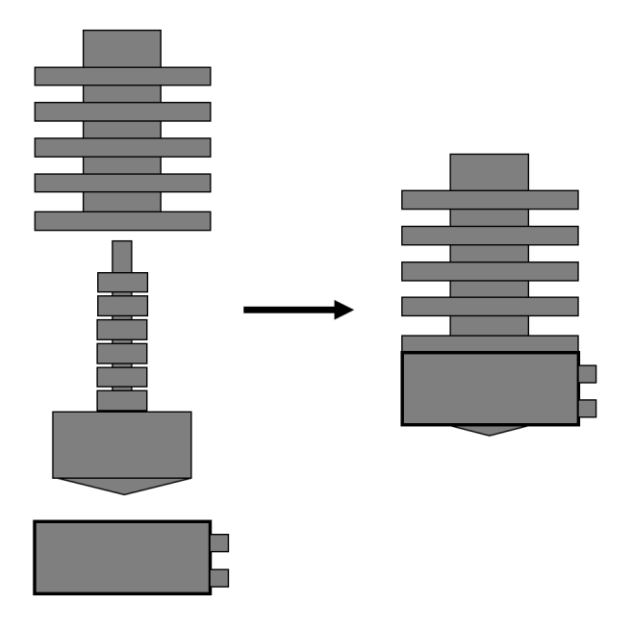


Figure 22. Illustration of thixo-printing nozzle design (Figure redrawn from Ref. (Lima *et al.* 2020)).

Material preparation in this experiment was found to be critical to the whole process. Mg-38Zn alloy was chosen as the printing material. Raw material ingots were extruded from 20 mm diameter to 5 mm diameter bars, then deformed to 1.75 mm diameter wires. A hydraulic press was used to handle both extrusion processes at 330°C under different loads. During the hot extrusion process, the material deformation can cause rupture of the original dendritic microstructure. After solidification, solid particles were found in the cross-sectional structure, corresponding to the globular morphology in the

semisolid state (Lima *et al.* 2020). Mg-38Zn filament was printed at 420°C. The filament inside the nozzle channel passes three temperature zone (shown in Figure 23): cold zone, transition zone, and hot zone. When the filament reaches the hot zone, a semisolid state material is formed and extruded out through a 1.0 mm nozzle, deposited on the substrate with a fixed 1.0 mm distance. Single and multilayer samples are illustrated in Figure 24.

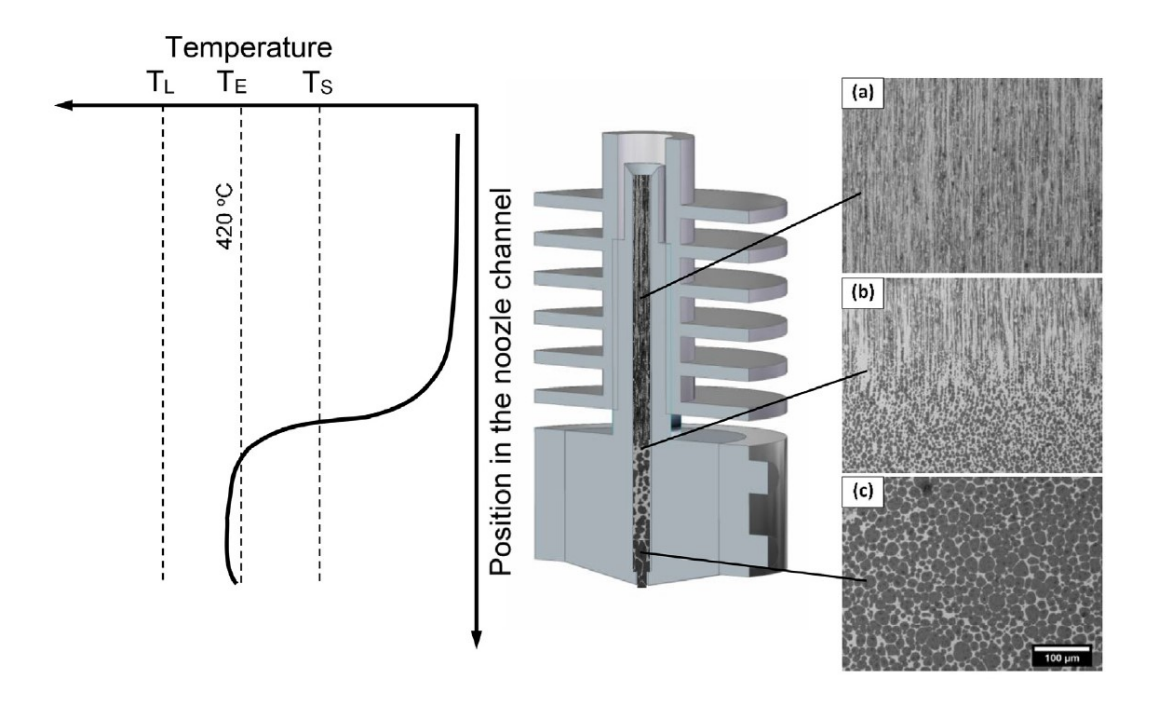


Figure 23. Schematic of microstructure evolution of tested alloy in channel flow through zones at different temperatures: (a) cold zone, (b) transition zone, and (c) hot zone; where T_L = liquidus temperature, T_E = extrusion temperature, and T_S = solidus temperature. (Lima *et al.* 2020)

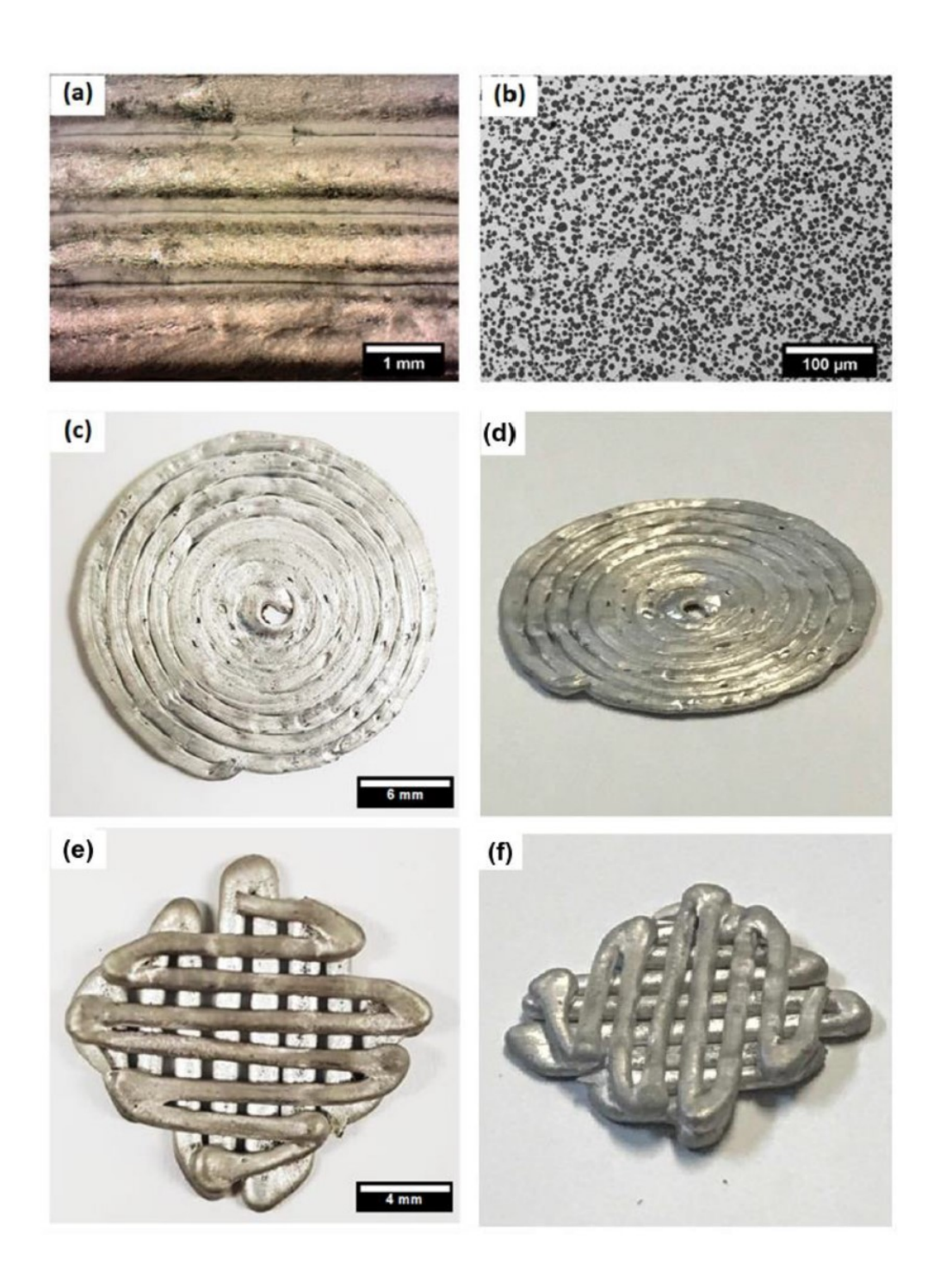


Figure 24. multilayer of printed sample. (b) Microstructure of Mg-38Zn filament. (c)-(f): Printed samples by semisolid FFF. (Lima *et al.* 2020)

5. Discussion and future work

Thixotropy is a reversible, time-dependent property that has been identified as a key to the refinement of material microstructure. Semisolid metal slurries obtained from the thixotropic process can improve the alloy's microstructure and optimize the metal

casting process. Previous modeling and simulation work on SSM mainly concentrated on modeling of semisolid rheology of different metals/alloys and simulation of semisolid slurries as a non-Newtonian fluid flowing in a simple channel. Existing research on thixotropic metal printing has demonstrated a possible method to melt and print metallic materials directly rather than process through a complicated powderbased printing system. However, currently available thixotropic printing systems are still in the infancy stage and are incapable of bridging the gap between the lab and manufacturing industries. Most of the thixotropic printing systems are facing the challenge of printing complex 3D geometry. Until recently, there is no clear indication that the major process parameters in thixotropic printing are fully understood and well controllable. Besides, tested metallic materials in most experiments were limited to low melting point alloys. For common metals used in manufacturing such as steel, aluminum-based alloy, and bio-friendly alloys, the printability remains unknown. On the other hand, these challenges on thixotropic printing, in turn, provide new opportunities for SSM study and system design. An integrated SSM processing/printing method, including heating, mixing, shearing, and extrusion, needs to be developed to provide better controllability over printing quality and fit realistic industrial-scale manufacturing. More quantitative analysis of major process parameters such as solid fraction during printing, shear rate at the nozzle, and cooling rate around the printing region need to be addressed. Moreover, thixotropic processability of metallic materials, especially printability of bio-friendly alloys, should be carefully explored in future investigations.

6. Summary and conclusion

This paper aims to review the general information of thixotropy, semi-solid metal processing, and the current development of thixotropic based metal 3D printing.

Semisolid processes can provide a venue for precise modeling control of metals from raw solid material to globular microstructure slurry. However, unlike SSP technologies for molding, casting and forging, thixotropic metal 3D printing is still in an infancy state and significant progress is yet awaited. The study of printing parameters and the development of capable printing systems are among main endeavors of current research. Nevertheless, the literature survey provided in this review paper demonstrates that the thixotropy of metals offers great opportunities for the development of new low-cost, high-quality 3D printing systems for metal 3D printing. The combination of SSM processing and 3D printing would potentially have positive impacts on today's manufacturing industries, although some technical challenges should be overcome to remove roadblocks to ultimate success.

Reference

- Abdulhameed, O., A. Al-Ahmari, W. Ameen and S.H. Mian. 2019. Additive manufacturing: Challenges, trends, and applications. *Advances in Mechanical Engineering* 11, no 2: 1687814018822880.
- Apelian, D., Y. Tsutsui, M. Kiuchi and K. Ichikawa. 2002. Semi-solid processing routes and microstructure evolution. In *Proc. 7th Int. Conf. on 'Semi-solid processing of alloys and composites'*, *Tsukuba*, *Japan*, 25-30.
- Atkinson, H. 2005. Modelling the semisolid processing of metallic alloys. *Progress in materials science* 50, no 3: 341-412.
- Barnes, H.A. 1997. Thixotropy—a review. *Journal of Non-Newtonian Fluid Mechanics* 70, no 1-2: 1-33.
- Barnes, H.A., J.F. Hutton and K. Walters. 1989. *An introduction to rheology*. Vol. 3 of: Elsevier.
- Blair, G.S. and F. Coppen. 1942. The subjective conception of the firmness of soft materials. *The American Journal of Psychology*: 215-29.
- Buschow, K.J., R.W. Cahn, M.C. Flemings, B. Ilschner, E.J. Kramer and S. Mahajan. 2001. Encyclopedia of materials. *Science and technology* 1: 11.
- Canyook, R., J. Wannasin, S. Wisuthmethangkul and M. Flemings. 2012.

 Characterization of the microstructure evolution of a semi-solid metal slurry during the early stages. *Acta Materialia* 60, no 8: 3501-10.
- Chen, W., L. Thornley, H.G. Coe, S.J. Tonneslan, J.J. Vericella, C. Zhu, E.B. Duoss,R.M. Hunt, M.J. Wight and D. Apelian. 2017. Direct metal writing: Controlling the rheology through microstructure. *Applied Physics Letters* 110, no 9: 094104.
- Chhabra, R.P. and J.F. Richardson. 1999. *Non-newtonian flow in the process industries:* Fundamentals and engineering applications: Butterworth-Heinemann.
- Chhabra, R.P. and J.F. Richardson. 2011. *Non-newtonian flow and applied rheology:*Engineering applications: Butterworth-Heinemann.
- Cotterill, R. 2003. Biophysics: An introduction: American Association of Physics Teachers.
- Darvell, B.W. 2018. Materials science for dentistry: Woodhead publishing.
- De Figueredo, A. 2001. Science and technology of semi-solid metal processing: North American Die Casting Assoc.

- De Souza Mendes, P.R. and R.L. Thompson. 2012. A critical overview of elasto-viscoplastic thixotropic modeling. *Journal of Non-Newtonian Fluid Mechanics* 187: 8-15.
- Fan, Z. 2002. Semisolid metal processing. *International materials reviews* 47, no 2: 49-85.
- Fan, Z. and J. Chen. 2002. Modelling of rheological behaviour of semisolid metal slurries part 2–steady state behaviour. *Materials Science and Technology* 18, no 3: 243-49.
- Fang, X., J. Du, Z. Wei, X. Wang, P. He, H. Bai, B. Wang, J. Chen, R. Geng and B. Lu. 2016. Study on metal deposit in the fused-coating based additive manufacturing. *Procedia Cirp* 55: 115-21.
- Flemings, M., R. Riek and K. Young. 1976. Rheocasting. *Materials Science and Engineering* 25: 103-17.
- Flemings, M.C. 1974. Solidification processing. *Metallurgical transactions* 5, no 10: 2121-34.
- Flemings, M.C. 1991. Behavior of metal alloys in the semisolid state. *Metallurgical transactions A* 22, no 5: 957-81.
- Frazier, W.E. 2014. Metal additive manufacturing: A review. *Journal of Materials Engineering and Performance* 23, no 6: 1917-28.
- Freundlich, H. and H. Röder. 1938. Dilatancy and its relation to thixotropy. *Transactions of the Faraday Society* 34: 308-16.
- Gao, W., Y. Zhang, D. Ramanujan, K. Ramani, Y. Chen, C.B. Williams, C.C. Wang,
 Y.C. Shin, S. Zhang and P.D. Zavattieri. 2015. The status, challenges, and future of additive manufacturing in engineering. *Computer-Aided Design* 69: 65-89.
- Goodeve, C. and G. Whitfield. 1938. The measurement of thixotropy in absolute units. *Transactions of the Faraday Society* 34: 511-20.
- Goodeve, C.F. 1939. A general theory of thixotropy and viscosity. *Transactions of the Faraday Society* 35: 342-58.
- Haga, T. and P. Kapranos. 2002. Simple rheocasting processes. *Journal of Materials Processing Technology* 130: 594-98.
- Hashmi, S. 2014. Comprehensive materials processing: Newnes.

- Jabbari, A. and K. Abrinia. 2018. A metal additive manufacturing method: Semi-solid metal extrusion and deposition. *The International Journal of Advanced Manufacturing Technology* 94, no 9-12: 3819-28.
- Jabbari, A. and K. Abrinia. 2019. Preparing a solid filament for use in additive manufacturing of metals. *JoM* 71, no 3: 1088-94.
- Ji, S., Z. Fan and X. Fang. 2002. Twin-screw rheomoulding of az91d mg-alloys.
- Joly, P. and R. Mehrabian. 1976. The rheology of a partially solid alloy. *Journal of Materials Science* 11, no 8: 1393-418.
- Kaufmann, H. and P.J. Uggowitzer. 2001. Fundamentals of the new rheocasting process for magnesium alloys. *Advanced engineering materials* 3, no 12: 963-67.
- Kaufmann, H., H. Wabusseg and P.J. Uggowitzer. 2000. Metallurgical and processing aspects of the nrc semi-solid casting technology. *ALUMINIUM-DUSSELDORF THEN ISERNHAGEN-* 76, no 1/2: 70-74.
- Kirkwood, D. 1994. Semisolid metal processing. *International materials reviews* 39, no 5: 173-89.
- Kobelev, V. and K.S. Schweizer. 2005. Dynamic yielding, shear thinning, and stress rheology of polymer-particle suspensions and gels. *The Journal of chemical physics* 123, no 16: 164903.
- Kopp, R., D. Neudenberger and G. Winning. 2001. Different concepts of thixoforging and experiments for rheological data. *Journal of Materials Processing Technology* 111, no 1-3: 48-52.
- Kumar, S.D., J. Ghose and A. Mandal. 2019. Thixoforming of light-weight alloys and composites: An approach toward sustainable manufacturing. In *Sustainable engineering products and manufacturing technologies*, 25-43: Elsevier.
- Larson, R.G. and Y. Wei. 2019. A review of thixotropy and its rheological modeling. *Journal of Rheology* 63, no 3: 477-501.
- Lashkari, O. and R. Ghomashchi. 2007. The implication of rheology in semi-solid metal processes: An overview. *Journal of Materials Processing Technology* 182, no 1-3: 229-40.
- Lima, D.D., K.N. Campo, S.T. Button and R. Caram. 2020. 3d thixo-printing: A novel approach for additive manufacturing of biodegradable mg-zn alloys. *Materials & design* 196: 109161.
- Liu, T.Y. 2002. Rheology of semisolid alloys under rapid change in shear rate.

- Mewis, J. 1979. Thixotropy-a general review. *Journal of Non-Newtonian Fluid Mechanics* 6, no 1: 1-20.
- Mewis, J. and N.J. Wagner. 2009. Thixotropy. *Advances in Colloid and Interface Science* 147: 214-27.
- Mewis, J. and N.J. Wagner. 2012. *Colloidal suspension rheology*: Cambridge University Press.
- Modigell, M. and J. Koke. 1999. Time-dependent rheological properties of semi-solid metal alloys. *Mechanics of Time-Dependent Materials* 3, no 1: 15-30.
- Mohammed, M., M. Omar, M. Salleh, K. Alhawari and M. Abdelgnei. 2014. An overview of semi-solid metal processing. *Australian Journal of Basic and Applied Sciences* 8, no 19: 369-73.
- Mohammed, M., M.Z. Omar, J. Syarif, Z. Sajuri, M. Salleh and K. Alhawari. 2013.

 Microstructural evolution during dprm process of semisolid ledeburitic d2 tool steel. *The Scientific World Journal* 2013.
- Mujumdar, A., A.N. Beris and A.B. Metzner. 2002. Transient phenomena in thixotropic systems. *Journal of Non-Newtonian Fluid Mechanics* 102, no 2: 157-78.
- Ngo, T.D., A. Kashani, G. Imbalzano, K.T. Nguyen and D. Hui. 2018. Additive manufacturing (3d printing): A review of materials, methods, applications and challenges. *Composites Part B: Engineering* 143: 172-96.
- Nguyen, Q. and P. Uhlherr. 1985. Thixotropic behavior of concentrated red mud suspensions. In *Journal of Rheology*, 815-15: AMER INST PHYSICS CIRCULATION FULFILLMENT DIV, 500 SUNNYSIDE BLVD, WOODBURY
- Nishimatsu, C. and J. Gurland. 1958. Experimental survey of the deformation of a hard-ductile two-phase alloy syste (wc-co: BROWN UNIV PROVIDENCE RI.
- Omar, M.Z., E. Palmiere, A. Howe, H. Atkinson and P. Kapranos. 2005. Thixoforming of a high performance hp9/4/30 steel. *Materials Science and Engineering: A* 395, no 1-2: 53-61.
- Pan, Q., D. Apelian and A.N. Alexandrou. 2004. Yield behavior of commercial al-si alloys in the semisolid state. *Metallurgical and materials transactions B* 35, no 6: 1187-202.
- Peterfi, T. 1927. Arch entwicklungsmech. Organ 112: 680.

- Polmear, I., D. Stjohn, J.-F. Nie and M. Qian. 2017. *Light alloys: Metallurgy of the light metals*: Butterworth-Heinemann.
- Püttgen, W., W. Bleck, G. Hirt and H. Shimahara. 2007. Thixoforming of steels—a status report. *Advanced engineering materials* 9, no 4: 231-45.
- Quaak, C., L. Katgerman and W. Kool. 1996. Viscosity evolution of partially solidified aluminium slurries after a shear rate jump. In *Proc. 4th Int. Conf. on SS Processing of Alloys and Composites*, 35-9.
- Riecker, S., J. Clouse, T. Studnitzky, O. Andersen and B. Kieback. 2016. Fused deposition modeling-opportunities for cheap metal am. *World PM2016-AM-Deposition Technologies*.
- Roussel, N. 2006. A thixotropy model for fresh fluid concretes: Theory, validation and applications. *Cement and concrete research* 36, no 10: 1797-806.
- Tanner, R.I. and K. Walters. 1998. Rheology: An historical perspective: Elsevier.
- Tzimas, E. and A. Zavaliangos. 2000. Evolution of near-equiaxed microstructure in the semisolid state. *Materials Science and Engineering: A* 289, no 1-2: 228-40.
- Uggowitzer, P., G. Gullo and A. Wahlen. 2000. Vom werkstoff zum bauteilsystem. *LKR-verlag Ranshofen*: 95.
- Underwood, E.E. 1970. Quantitative stereology. *Reading, MA*: 5.
- Wagner, M.A., A. Hadian, T. Sebastian, F. Clemens, T. Schweizer, M. Rodriguez-Arbaizar, E. Carreño-Morelli and R. Spolenak. 2021. Fused filament fabrication of stainless steel structures-from binder development to sintered properties.

 *Additive Manufacturing: 102472.
- Wei, Y., M.J. Solomon and R.G. Larson. 2019. Time-dependent shear rate inhomogeneities and shear bands in a thixotropic yield-stress fluid under transient shear. *Soft matter* 15, no 39: 7956-67.
- Zhang, Y., Y. Zhang, W. She, L. Yang, G. Liu and Y. Yang. 2019. Rheological and harden properties of the high-thixotropy 3d printing concrete. *Construction and Building Materials* 201: 278-85.

List of Figures

Figure 1. Time dependent relation of thixotropy for a red mud suspension (59wt% solid
content) (Chhabra and Richardson 2011)
Figure 2. Schematic view of shear stress versus shear rate for thixotropic and rheopectic
fluids. (Figure redrawn from Ref. (Chhabra and Richardson 2011))
Figure 3. Example of the formation of thixotropy in an aqueous particulate suspension.
Interparticle hydrogen bonding can cause the formation of a reversible gel network.
(Figure redrawn from Ref. (Darvell 2018))
Figure 4. Solidified alloy structure: (a) dendritic microstructure typically observed in as-
cast samples; and (b) globular microstructure in semisolid alloy samples (Atkinson
2005)
Figure 5. Evolution of shear stress for a thixotropic material subject to step changes of
shear rate. (Figure redrawn from Ref. (Barnes et al. 1989))
Figure 6. Apparent viscosity vs. fraction solid (fs) of Sn-15 wt.% Pb sheared
continuously and cooled at 0.33 K/min at different shear rates (after Joly and Mehrabian
1976) (Merton C Flemings 1991; Joly and Mehrabian 1976)
Figure 7. Apparent viscosity of Sn–15% Pb slurries under different shear rate ($\gamma = 115$
s-1,(γ)=230 s-1, and γ =350 s-1). Samples were shared then kept at solid fraction of
0.45 and 0.50. (Joly and Mehrabian 1976)
Figure 8. (a) Solid fraction of 356 aluminum alloy at different rheocasting times. (b)
Total solid particles and the related particle density at different rheocasting times.
(Canyook et al. 2012)
Figure 9. Simulation results of a casting process with a Newtonian fluid and a
thixotropic non-Newtonian fluid (Modigell and Koke 1999)

Figure 10. Schematic diagrams of methods for producing nondendritic structures: (a)
batch stirring, (b) continuous stirring and extrusion, and (c) electromagnetic stirring
with continuous casting. (Figure redrawn from Ref. (Merton C Flemings 1991)) 19
Figure 11. Rheocasting processes: (a) process using a cooling slope, and (b) process
using low superheat casting. (Figure redrawn from Ref. (Haga and Kapranos 2002)) 21
Figure 12. Schematic of (A) rheocasting method and (B) thixoforming method. (Figure
redrawn from Refs. (Fan and Chen 2002; Kirkwood 1994; Kumar et al. 2019)) 22
Figure 13. Schematic of a thixomolding machine for producing injection molded
magnesium alloy components. (Figure redrawn from Ref. (Polmear et al. 2017)) 23
Figure 14. Principle of fused-coating based AM. (Figure redrawn from Ref. (Fang et al.
2016))
Figure 15. Schematic diagram of fused-coating based AM. (Figure redrawn from Ref.
(Fang et al. 2016))
Figure 16. Metal parts fabricated by FCAM process. (Fang et al. 2016)
Figure 17. The extrusion dies set (left), deformation zone (up right), and produced wire
(down right). (Jabbari and Abrinia 2018)
Figure 18. Schematic diagram of Developed SSMED thixo-extruder. (Figure redrawn
from Ref. (Jabbari and Abrinia 2018))
Figure 19. Deposited layers of semisolid alloy. A) Four layers printed adjacent to each
other. B) Thixo-extruder printing a sample. C) A printed single layer square shape. D) A
three layers printed sample. (Jabbari and Abrinia 2018)
three layers printed sample. (Jabbari and Abrinia 2018)
Figure 20. Schematic diagram of the DMW system comprised of an upper reservoir

Figure 21. DMW fabricated Bi/5Sn25 structures and their microstructures. The
characteristic feature size of the filament is close to the nozzle size. (a) "Zigzag" pattern
printed at 200°C. (b) Two layered lattice structure with overhanging features (blue
inset) printed at 190°C. (c) and (d) Filament microstructures of prints (a) and (b),
respectively, exhibiting a mixture of polygonal Bi blocks and the Bi-Sn eutectic matrix.
(e) A Bi75Sn25 filament printed at 200°C without shear. Many long need-like dendrites
tend to clog the nozzle and hence prevent steady state printing. (Chen et al. 2017) 30
Figure 22. Illustration of thixo-printing nozzle design (Figure redrawn from Ref. (Lima
et al. 2020))
Figure 23. Schematic of microstructure evolution of tested alloy in channel flow
through zones at different temperatures: (a) cold zone, (b) transition zone, and (c) hot
zone; where T_L = liquidus temperature, T_E = extrusion temperature, and T_S = solidus
temperature. (Lima et al. 2020)
Figure 24. multilayer of printed sample. (b) Microstructure of Mg-38Zn filament. (c)-
(f): Printed samples by semisolid FFF. (Lima et al. 2020)